Characterizing the Influence of Abstraction in Full-Scale Wind Turbine Nacelle Testing

Preprint

Ryan Schkoda and Amin Bibo
Clemson University Restoration Institute

Yi Guo, Scott Lambert, and Robb Wallen
National Renewable Energy Laboratory

To be presented at the ASME 2016 International Design Engineering Technical Conferences and Computers and Information in Engineering Conference (IDETC2016)
Charlotte, North Carolina
August 21–24, 2016

NREL is a national laboratory of the U.S. Department of Energy
Office of Energy Efficiency & Renewable Energy
Operated by the Alliance for Sustainable Energy, LLC

This report is available at no cost from the National Renewable Energy Laboratory (NREL) at www.nrel.gov/publications.

Conference Paper
NREL/CP-5000-66302
August 2016

Contract No. DE-AC36-08GO28308

NOTICE

The submitted manuscript has been offered by an employee of the Alliance for Sustainable Energy, LLC (Alliance), a contractor of the US Government under Contract No. DE-AC36-08GO28308. Accordingly, the US Government and Alliance retain a nonexclusive royalty-free license to publish or reproduce the published form of this contribution, or allow others to do so, for US Government purposes.

This report was prepared as an account of work sponsored by an agency of the United States government. Neither the United States government nor any agency thereof, nor any of their employees, makes any warranty, express or implied, or assumes any legal liability or responsibility for the accuracy, completeness, or usefulness of any information, apparatus, product, or process disclosed, or represents that its use would not infringe privately owned rights. Reference herein to any specific commercial product, process, or service by trade name, trademark, manufacturer, or otherwise does not necessarily constitute or imply its endorsement, recommendation, or favoring by the United States government or any agency thereof. The views and opinions of authors expressed herein do not necessarily state or reflect those of the United States government or any agency thereof.

This report is available at no cost from the National Renewable Energy Laboratory (NREL) at www.nrel.gov/publications.

Available electronically at SciTech Connect http:/www.osti.gov/scitech

Available for a processing fee to U.S. Department of Energy and its contractors, in paper, from:

U.S. Department of Energy
Office of Scientific and Technical Information
P.O. Box 62
Oak Ridge, TN 37831-0062
OSTI http://www.osti.gov
Phone: 865.576.8401
Fax: 865.576.5728
Email: reports@osti.gov

Available for sale to the public, in paper, from:

U.S. Department of Commerce
National Technical Information Service
5301 Shawnee Road
Alexandria, VA 22312
NTIS http://www.ntis.gov
Phone: 800.553.6847 or 703.605.6000
Fax: 703.605.6900
Email: orders@ntis.gov

Cover Photos by Dennis Schroeder: (left to right) NREL 26173, NREL 18302, NREL 19758, NREL 29642, NREL 19795.

NREL prints on paper that contains recycled content.

Proceedings of ASME 2016 International Design Engineering Technical Conferences and Computers and Information in Engineering Conference
IDETC2016
August 21–24, 2016, Charlotte, North Carolina, USA

IDETC2016-60275

CHARACTERIZING THE INFLUENCE OF ABSTRACTION IN FULL-SCALE WIND TURBINE NACELLE TESTING

Ryan Schkoda*, Amin Bibo

Clemson University Wind Turbine Drivetrain Testing Facility
Clemson University Restoration Institute
North Charleston, South Carolina 29405
Email: schkoda@clemson.edu
Email: abibo@clemson.edu

Yi Guo, Scott Lambert, and Robb Wallen

National Wind Technology Center
National Renewable Energy Laboratory
Golden, Colorado 80303
Email: Yi.Guo@nrel.gov
Email: Scott.Lambert@nrel.gov
Email: Robb.Wallen@nrel.gov

ABSTRACT

In recent years, there has been a growing interest in full-scale wind turbine nacelle testing to complement individual component testing. As a result, several wind turbine nacelle test benches have been built to perform such testing with the intent of loading the integrated components as they are in the field. However, when mounted on a test bench the nacelle is not on the top of a tower and does not have blades attached to it—this is a form of abstraction. This paper aims to quantify the influence of such an abstraction on the dynamic response of the nacelle through a series of simulation case studies. The responses of several nacelle components are studied including the main bearing, main shaft, gearbox supports, generator, and yaw bearing interface. Results are presented to highlight the differences in the dynamic response of the nacelle caused by the abstraction. Additionally, the authors provide recommendations for mitigating the effects of the abstraction.

INTRODUCTION

Several wind turbine nacelle test laboratories in the United States and Europe have equipment to perform mechanical and electrical testing of wind turbine nacelles ranging from less than 1 MW to 20 MW in size [1–6]. The term nacelle refers to the enclosure at the top of a wind turbine's tower and all the components inside of it including the main shaft, main bearing, main frame or bedplate, gearbox, high-speed coupling, generator, and yaw interface as depicted in Fig. 1 (which shows a multibody model based on a GE 1.6-100 wind turbine nacelle).

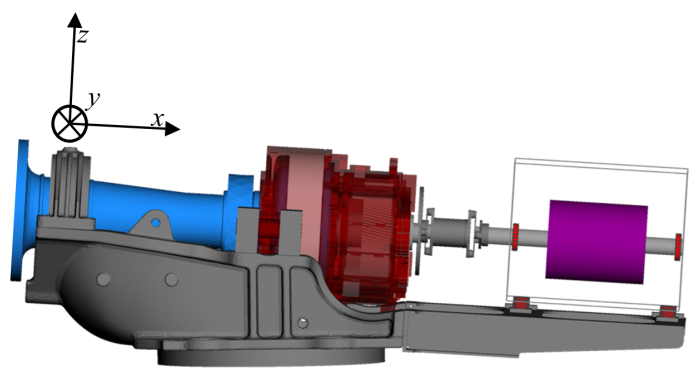

FIGURE 1: Profile view of the drivetrain used to study the influence of abstraction. Image captured by Ryan Schkoda from SIMPACK.

These nacelle facilities are not wind tunnels. They generally consist of mechanical dynamometers with the added ability to apply nontorque loads to the nacelle's main shaft and some

*Address all correspondence to this author.

This report is available at no cost from the National Renewable Energy Laboratory (NREL) at www.nrel.gov/publications.

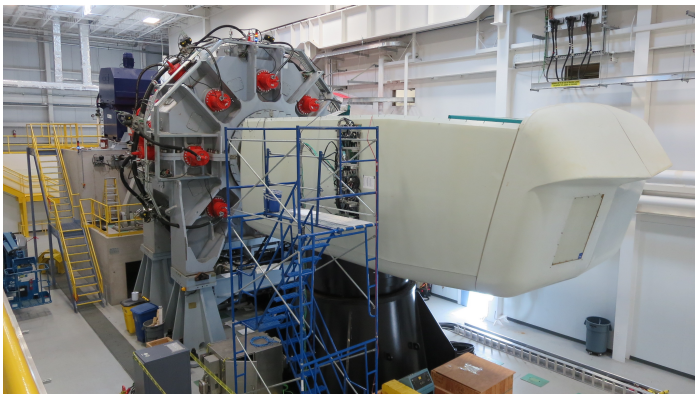

FIGURE 2: Photograph of a nacelle installed on Clemson University's 7.5-MW test bench. Photograph taken by Ryan Schkoda.

type of electrical grid simulator for realistic emulation of electrical loads. As such, the nacelle and down-tower assembly (grid interface power electronics) are installed on the test bench and tested without blades or a tower, as shown in Fig. 2. This paper describes the effect that the absence of the blades and tower has on the dynamic response of the nacelle.

ANALYSIS APPROACH

The abstraction is strictly related to the absence of the blades and tower. As such, the influence of abstraction is independent of the test bench and the influence of the test bench must be addressed separately. The analysis approach in this paper quantifies the influence of abstraction independent of the test bench by using simulation tools to study the device under test in isolation (Fig. 3). In this configuration, the nacelle is mounted to an "ideal test bench." The nacelle is fixed to a rigid floor and is acted upon by a six-dimensional load vector with infinite bandwidth at the main shaft interface and by an ideal air gap torque in the generator, again, with infinite bandwidth. This is impossible in reality, but achievable in simulation allowing for the influence of abstraction to be studied independently. A next step is to include the test bench in the analysis and determine how the nacelle's response is further influenced by the presence of the test bench components.

A diagram of the analysis steps is shown in Fig. 4. In the case of nacelle testing, the system input consists of a wind field and grid conditions. This input may be constant or time varying. The input is applied to the full wind turbine and a full system response is captured. From this full system response, the hub loads and generator torque are extracted and applied to the abstracted nacelle. Finally, the subsystem response of the full turbine is compared to the corresponding response from the abstracted nacelle and test bench model.

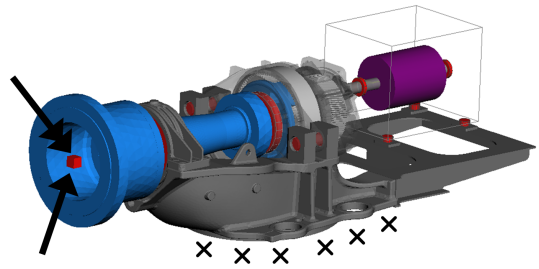

FIGURE 3: Ideal test bench configuration. Nacelle is rigidly attached to the ground and the hub point loads are controlled perfectly. Image captured by Ryan Schkoda from SIMPACK.

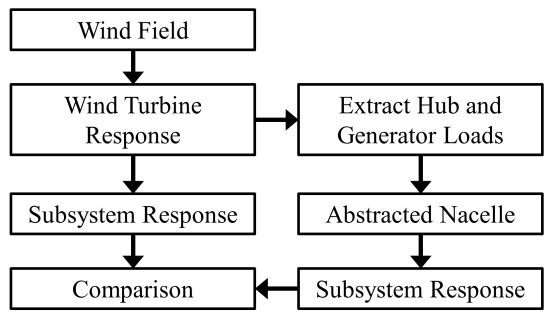

FIGURE 4: Diagram of the analysis methodology.

MODEL DESCRIPTION

The analysis presented in this paper is based on a simulation of a full wind turbine as well as the nacelle in isolation. Researchers from Clemson University and the National Renewable Energy Laboratory (NREL) have developed various dynamic models to study the influence of abstraction. This section elaborates on the specific models used in this study. NREL researchers developed reduced-order, lumped-parameter pure torsional models to perform modal surveys and calculate system dynamic responses in real time. Clemson researchers developed multibody dynamic models in SIMPACK for comprehensive load path analysis. For detailed descriptions of the Clemson test equipment/test benches, see [7].

Lumped-Parameter Models

Three reduced-order lumped-parameter models were established to provide fast solutions of the torsional assembly's dynamic response and modal survey. These models are: (1) wind turbine rotor and test article assembly (WT model), (2) test article only, and (3) test bench and test article assembly (Dyno model). Figure 5 shows the torsional model representation of NREL's 5-MW dynamometer test bench and test article assembly model. The figure includes the dynamometer drive motor, dynamometer drive gearbox, nontorque load system, test article

This report is available at no cost from the National Renewable Energy Laboratory (NREL) at www.nrel.gov/publications.

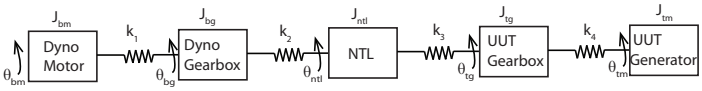

FIGURE 5: Block diagram of the torsional drivetrain model used to derive the mathematical model. UUT stand for unit under test.

gearbox, and test article generator. Subcomponents of these gearboxes, motor, and generator are not included in the model.

The final form of the Dyno model is given by

$$\tilde{J}\ddot{X} + \tilde{C}\dot{X} + \tilde{K}X = \tilde{T}, \tag{1}$$

where

$$\begin{aligned}\tilde{J} &= diag\{J_{bm}, J_{bg}, J_{ntl}, J_{tg}, J_{tm}\}\\ \tilde{C} &= diag\{C_{bm}, C_{bg}, C_{ntl}, C_{tg}, C_{tm}\}\\ \tilde{X} &= diag\{\theta_{bm}, \theta_{bg}, \theta_{ntl}, \theta_{tg}, \theta_{tm}\}.\end{aligned}$$

The external forces of the system are

$$\tilde{T} = diag\{T_{bm}, 0, 0, 0, T_{tm}\},$$

and the stiffness matrix

$$\tilde{K} = \begin{bmatrix} k_1 & -k_1 & 0 & 0 & 0\\ -k_1 & k_1+k_2 & -k_2 & 0 & 0\\ 0 & -k_2 & k_2+k_3 & -k_3 & 0\\ 0 & 0 & -k_3 & k_3+k_4 & -k_4\\ 0 & 0 & 0 & -k_4 & k_4 \end{bmatrix}. \tag{2}$$

The derivation of the Dyno model is in the Appendix. The other two models have been established in a similar fashion but their derivations are excluded for brevity.

Multibody-Dynamics Models

Two multibody configurations were established to study the full wind turbine response and the abstracted nacelle response: (1) the abstracted nacelle model, and (2) the full wind turbine model. In both configurations, the nacelle was modeled after a GE 1.6-100 machine head (see Fig. 1). However, the lumped-parameter torsional model presented earlier is not based on it. The nacelle model is purely mechanical, neglecting any pitch, yaw, and generator torque control action, and is designed to capture the structural response of the nacelle.

The full wind turbine is shown in Fig. 6 and includes a flexible tower and blades, as well as the nacelle model. The wind profile required to drive the full turbine model is generated by using

FIGURE 6: Full turbine model used to generate truth data for the load path analysis. Image captured by Amin Bibo from SIMPACK.

TurbSim and the aerodynamic loads on the blades are calculated with AeroDyn. The blade and tower parameters are based on the FAST WindPact 1.5-MW certification test case wind turbine model in lieu of using GE proprietary data. This model is used to generate the truth data for the Clemson analysis.

RESULTS

The loading cases studied in this paper were based on design load cases outlined in International Electrotechnical Commission 61400-01 [8], as well as standard experimental load cases. Specifically, the load cases are normal power production, power production plus occurrence of fault, and generator torque steps.

The drivetrain component loads are studied using the multibody models during normal power production. The goal of this analysis is to understand how the abstraction of the nacelle affects the load path and dynamic content of drivetrain component loads. The lumped-parameter torsional model was used to study the main shaft's torque, speed, and torsional displacement during power production plus occurrence of fault (grid loss) and for the torque steps. The goal of this analysis is to determine to what

This report is available at no cost from the National Renewable Energy Laboratory (NREL) at www.nrel.gov/publications.

extent the torsional properties of the nacelle are influenced by its abstraction as well as the effects of having the nacelle coupled to the test bench in ways that do not affect field conditions.

Load Path Analysis During Power Production

The multibody model was used to study the nacelle's load path. In an effort to reduce the number of influencing factors, the blade pitch was kept constant throughout the simulation and the generator torque was slowly increased before being held constant. Figure 7 shows the component wind velocities at the hub center (a) and the extracted hub point loads (b). Figure 8 shows the extracted generator torque and the speed and power throughout the simulation. The loads in Fig. 7b and Fig. 8 were applied to the nacelle only model in order to generate the responses that are compared to the full wind turbine response. The comparisons are in Fig. 9-11.

Please note that the magnitude of the forces shown in these figures do not reflect the actual forces on a GE 1.6-100 wind turbine nacelle because of the assumptions made for the tower and blades (use of WindPACT data versus proprietary GE data), and constant blade pitch assumption (no pitch control). The loads shown in Fig. 9-Fig. 11 represent a similar class of wind turbine operating at constant pitch.

Figure 9 shows the main bearing loads calculated during the full turbine simulation compared to those resulting from the abstracted nacelle simulation (see Fig. 1 for the coordinate axis). The figure shows a significant difference in the load spectrum for the two scenarios. The F_x, or thrust direction, shows a decrease in low-frequency content around 0.25 Hz, as well as a modest increase in high-frequency content. The F_y, or lateral, and F_z, or vertical, components of the main bearing load show good agreement across the spectrum except for significant spikes between 5 Hz and 6 Hz. Results of modal analysis, not presented in this paper, show that these peaks are related to the pitch and yaw modes of the abstracted nacelle. Although the results may not be in full quantitative agreement with the field response because of damping and other model parameter uncertainties, the results show qualitative changes in the nacelle response as a result of the abstraction.

From a testing perspective, it is important to avoid exciting these newly introduced modes because of the possibility of arriving at an incorrect conclusion regarding component fatigue and life. This could be achieved by making sure that the hub loads are low-pass filtered before being applied to the abstracted nacelle.

A similar analysis was performed for the gearbox supports and the results are shown in Fig. 10. The vertical loads experienced by the gearbox supports were all but unaltered by the differing boundary conditions. In the full turbine, the gearbox was located near the center line of the tower, thereby giving the gearbox a relatively stiff support structure in the vertical direction. The fixed boundary provided a similarly stiff vertical support structure resulting in a similar vertical load profile.

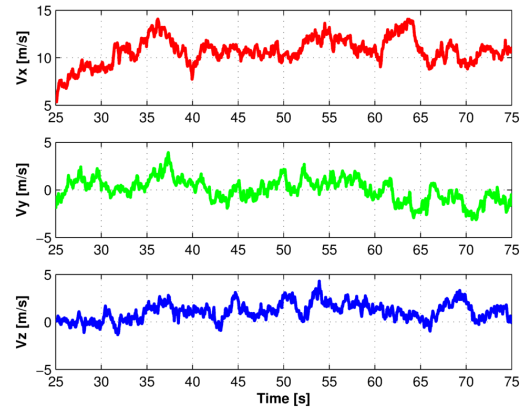

(a) Hub center wind velocities

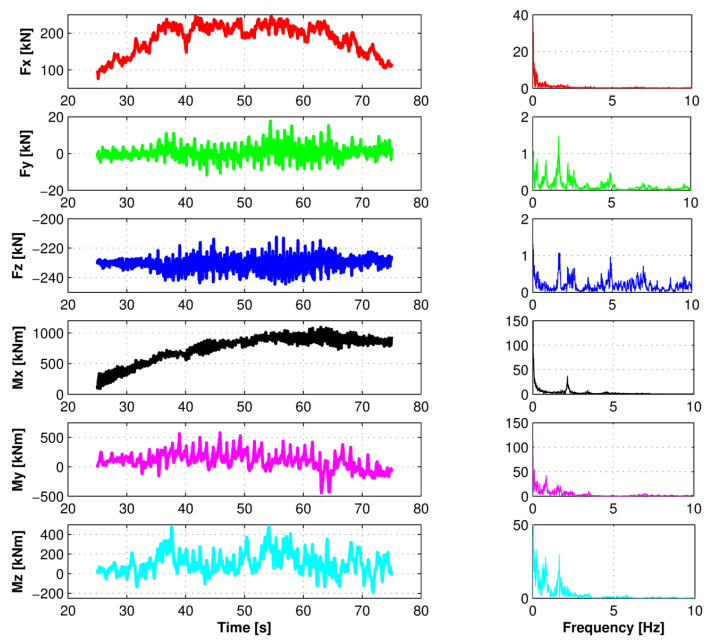

(b) Hub point loads

FIGURE 7: Component wind velocities at the hub center (a) and the resulting hub point loads (b).

The thrust and lateral loads revealed different load spectrums between the full turbine and abstracted nacelle in the higher frequency range wherein the abstracted nacelle shows spikes between 5 Hz and 6 Hz—similar to those observed in the main bearing analysis.

Finally, the analysis was performed for the tower interface, or yaw bearing loads, and the results are shown in Fig. 11. The results for the linear forces observed at the tower interface are similar to those of the main bearing, but not identical. The thrust direction saw a decrease in the low-frequency content and a moderate increase in high-frequency content. The lateral direction

This report is available at no cost from the National Renewable Energy Laboratory (NREL) at www.nrel.gov/publications.

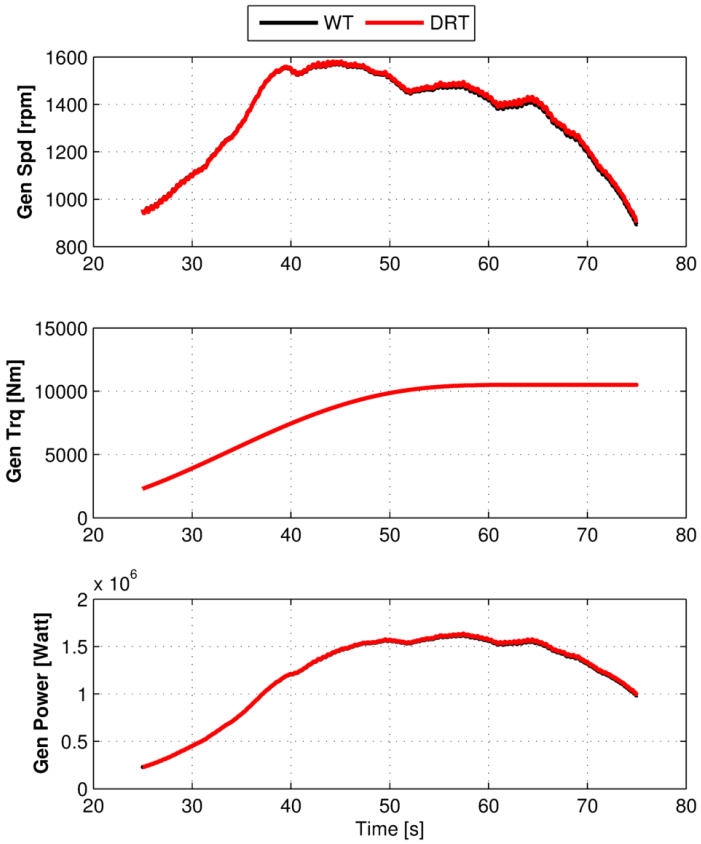

FIGURE 8: Generator loads.

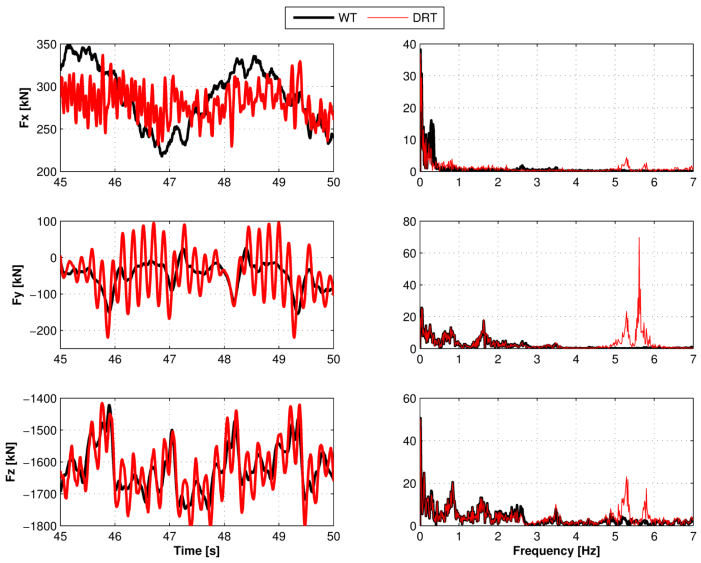

FIGURE 9: Main bearing loads.

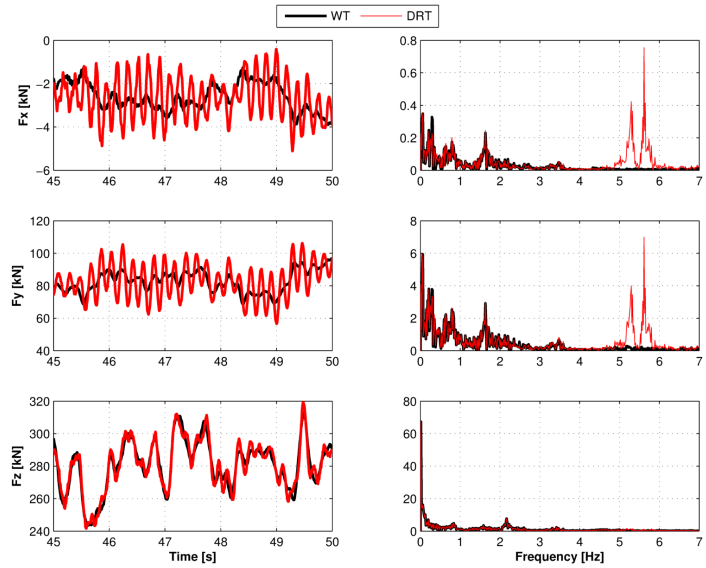

(a) Left-hand side

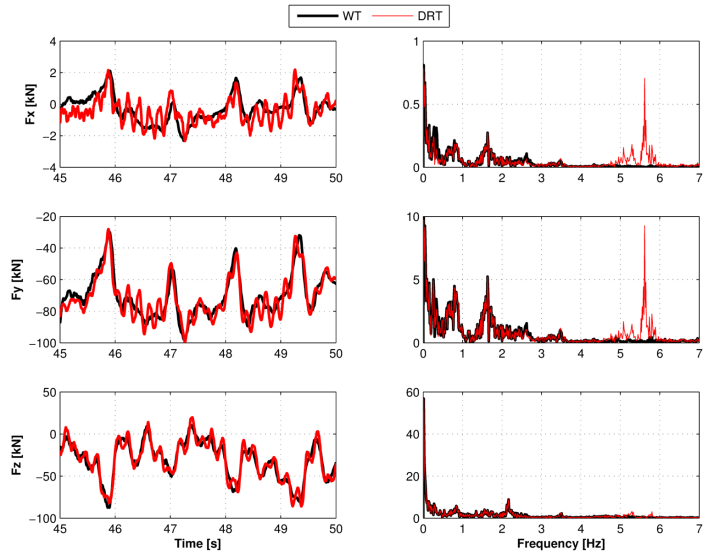

(b) Right-hand side

FIGURE 10: Gearbox support loads.

experiences a very significant increase in frequency content between 5 Hz and 6 Hz. The vertical direction shows perhaps the most overall distortion of any location. Not only is there additional frequency content between 5 Hz and 6 Hz but the peaks near 0.5 Hz and 2.5 Hz are subdued.

The results for the bending moments at the tower interface are much more uniform than any other group. The full turbine and abstracted nacelle have similar responses below 4 Hz with the addition of peaks between 5 Hz and 6 Hz.

Note that even with perfect controllability of the hub loads

This report is available at no cost from the National Renewable Energy Laboratory (NREL) at www.nrel.gov/publications.

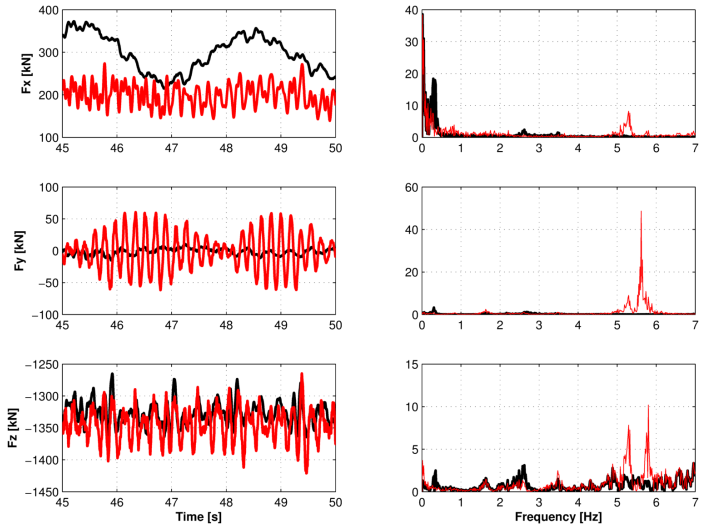

(a) Linear loads

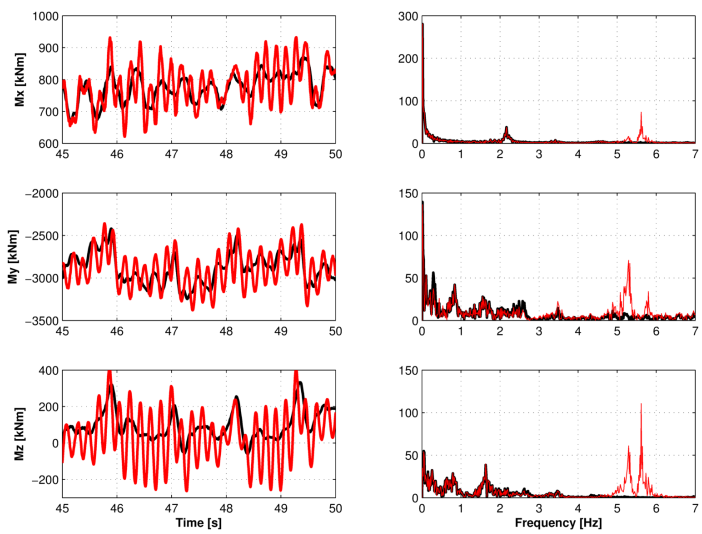

(b) Bending moments

FIGURE 11: Yaw bearing loads.

(ideal test bench) the component loads may not be as they are in the field. These differences are caused by differences in the physical configuration of the test bench when compared to the full nacelle and are present even in the ideal test bench scenario. This issue can be addressed by selectively modifying the input loads using load path analysis results.

Torsional Displacement During Transients

The lumped-parameter models were used to study both the influence of abstraction as well as the effects of coupling the nacelle to the test bench (nonideal or realistic test bench). Recall that the lumped-parameter model is based on a different nacelle than the multibody model. Two transient events are discussed in this section including a torque ramp and emergency stop. Torque ramps are one of the typical dynamometer test profiles but the emergency stop event differs from the field measurement. Using NREL's 5-MW dynamometer, a mechanical torque-limiting device built into the high-speed shaft is attached to the output of the drive motor. This device prevents the dynamometer from inducing excessive torque loads from a motor or test specimen fault, or other unusual transient condition. The torque limiter consists of five modules that can be engaged individually or adjusted to a lower setting if the maximum desired torque during testing is limited. The dynamometer emergency stop event was created by engaging a single module of the torque limiter while leaving the remaining four modules disengaged, and then gradually increasing the torque command until the device was activated.

The input torque during the torque ramp is shown in Figure 12 and Figure 14. The torsional dynamic responses of the test article generator during these events calculated using three aforementioned lumped-parameter models are shown in Figure 13 and Figure 15, respectively. The Dyno model calculated the highest displacement of the generator torsional response compared to other approaches because the overall assembly stiffness is reduced by the test bench compliance. The stiffness of the dynamometer test bench has the same order of magnitude of the test article, therefore, the equivalent stiffness of the test bench and test article assembly is a part of the test article. The stiffness between the wind turbine rotor and test article is much greater than the test article stiffness. Thus, the WT model prediction of the torsional displacement agrees with the test-article-only model. Moreover, the Dyno model calculated the highest torsional vibration (oscillations on the static values) of the generator than the other approaches. The inertia of the rotor in the WT model is nearly twice that of the dynamometer test bench, resulting in the lowest torsional vibration.

During the stop, torque in the system quickly dropped to zero and the reflected inertia and backlash in the system created torque reversals afterwards for about 10 s. As shown in Figure 15, the system oscillation lasted nearly 50 s after torque reduced to zero. The oscillation length is determined by the system impedance implemented in the model. Among the three models, the Dyno model predicted the largest oscillation because of relatively low inertia compared to the WT model (field condition); however, the overall vibration and displacement amplitudes during the torque transient were small compared to system backlash or tolerance.

Natural Frequencies

Eigenvalue analysis of a representative 3-MW-scale wind turbine drivetrain using the lumped-parameter models provided torsional natural frequencies and mode shapes of the studied systems. The natural frequencies were compared among various

This report is available at no cost from the National Renewable Energy Laboratory (NREL) at www.nrel.gov/publications.

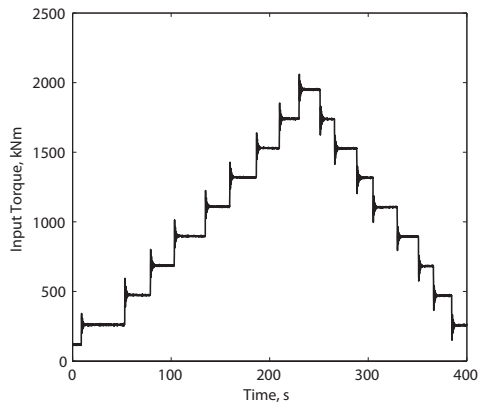

FIGURE 12: Drivetrain input torque during a torque step event.

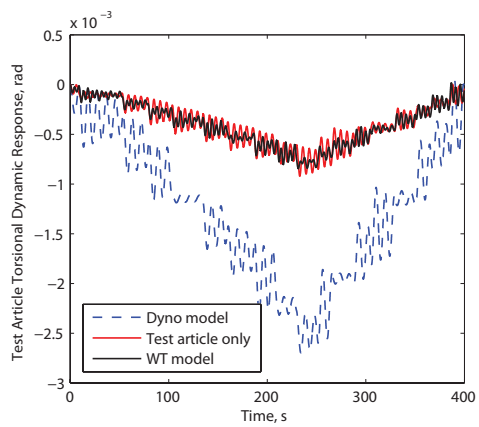

FIGURE 13: Test article generator torsional response during a torque step event.

models and experimental data at NREL's 5-MW dynamometer facility as shown in Table 1. The number of natural frequencies calculated by the models equals the number of degrees of freedom that each model has. Because each model calculates different numbers of natural frequencies, we focused only on the first drivetrain mode in this study. The first natural frequency of the test article is greater than the WT and Dyno models because both the dynamometer and wind turbine have large inertia from the drive motor and wind turbine blades. The Dyno model agrees reasonably with experimental data. Moreover, the WT model prediction is close to the model output of the Dyno model (within 10%), which suggests that the dynamometer test bench is able to reproduce the drivetrain torsional modal properties of the test article.

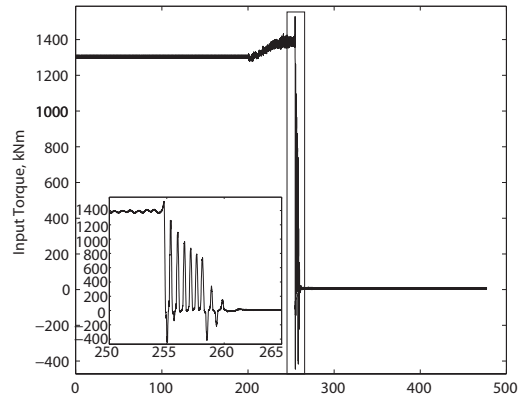

FIGURE 14: Drivetrain input torque during an emergency stop event.

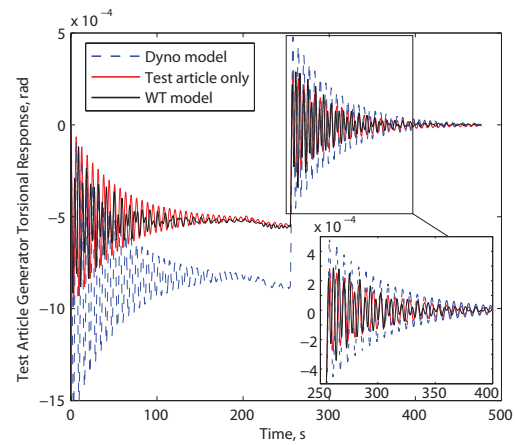

FIGURE 15: Test article generator torsional response during an emergency stop event.

TABLE 1: Torsional Natural Frequencies.

Frequency, Hz	Test article	WT	Dyno model	Experiment
1st	0.99	0.75	0.78	0.85
2nd	–	1.37	3.89	3.72
3rd	6.83	–	7.30	–
4th	–	27.35	24.68	28.50

CONCLUSION

A simulation-based study was performed to quantify the influence of abstraction on the dynamic response of a wind turbine nacelle. The dynamic multibody models presented in this study

This report is available at no cost from the National Renewable Energy Laboratory (NREL) at www.nrel.gov/publications.

were used to obtain the response of the full wind turbine model and the abstracted nacelle for different loading conditions. The influence of coupling the nacelle to the test bench on the torsional response is also studied with the help of the lumped-parameter torsional models. Results comparing the responses in the time and frequency domains are presented and discussed.

We found that the different boundary conditions experienced by the abstracted nacelle in the ideal test bench configuration have little to no effect on the lower frequency component loads. However, this abstraction introduces additional high-frequency content in the component loads that is not present in the full turbine response. As such, it is important to avoid exciting these newly introduced modes by low-pass filtering the input loads to accurately match the intended load profile. Failing to do so may lead to an incorrect conclusion regarding component fatigue and life. Despite the moderate influence of the abstraction on wind turbine nacelle loads, we anticipate a relatively strong influence on the dynamic displacement and vibration of the nacelle.

ACKNOWLEDGMENT

NREL researchers' work was funded under a Cooperative Research and Development Agreement between NREL and Clemson (CRD-13-509). This work was supported by the U.S. Department of Energy under Contract No. DE-AC36-08GO28308 with the National Renewable Energy Laboratory. Funding for the work was provided by the DOE Office of Energy Efficiency and Renewable Energy, Wind and Water Power Technologies Office.

APPENDIX: LUMPED-PARAMETER TORSIONAL MODEL DERIVATION

Lagrange's equations were derived for the studied assembly by carrying out the following steps. The kinematic energy of the system can be expressed as

$$T = \frac{1}{2}\left[J_{bm}\dot{\theta}_{bm}^2 + J_{bg}\dot{\theta}_{bg}^2 + J_{ntl}\dot{\theta}_{ntl}^2 + J_{tg}\dot{\theta}_{tg}^2 + J_{tm}\dot{\theta}_{tm}^2\right]. \quad (3)$$

The potential energy of the system is

$$V = \frac{1}{2}\left\{\begin{array}{c} k_1\left(\theta_{bm}-\theta_{bg}\right)^2 + k_2\left(\theta_{bg}-\theta_{ntl}\right)^2 + k_3\left(\theta_{ntl}-\theta_{tg}\right)^2 \\ +k_4\left(\theta_{tg}-\theta_{tm}\right)^2 \end{array}\right\}. \quad (4)$$

The final form of the Lagrangian $L = T - V$ can be expressed as

$$L = \frac{1}{2}\left\{\begin{array}{l} J_{bm}\dot{\theta}_{bm}^2 + J_{bg}\dot{\theta}_{bg}^2 + J_{ntl}\dot{\theta}_{ntl}^2 + J_{tg}\dot{\theta}_{tg}^2 + J_{tm}\dot{\theta}_{tm}^2 \\ -k_1\left(\theta_{bm}-\theta_{bg}\right)^2 - k_2\left(\theta_{bg}-\theta_{ntl}\right)^2 \\ -k_3\left(\theta_{ntl}-\theta_{tg}\right)^2 - k_4\left(\theta_{tg}-\theta_{tm}\right)^2 \end{array}\right\}. \quad (5)$$

The virtual work performed by the applied forces can be written as

$$\delta\bar{W}_{nc} = \delta\left(T_{bm}\theta_{bm} + T_{tm}\theta_{tm}\right) = T_{bm}\delta\theta_{bm} + T_{tm}\delta\theta_{tm}. \quad (6)$$

The expression

$$\frac{d}{dt}\left(\frac{\partial L}{\partial\dot{\theta}_{bm}}\right) - \frac{\partial L}{\partial\theta_{bm}} = \frac{\partial\bar{W}_{nc}}{\partial\theta_{bm}}$$

leads to

$$J_{bm}\ddot{\theta}_{bm} + C_{bm}\dot{\theta}_{bm} + k_1(\theta_{bm}-\theta_{bg}) = T_{bm}. \quad (7)$$

Following the same process, remaining equations of motion are derived as

$$J_{bg}\ddot{\theta}_{bg} + C_{bg}\dot{\theta}_{bg} - k_1(\theta_{bm}-\theta_{bg}) + k_2(\theta_{bg}-\theta_{ntl}) = 0 \quad (8)$$

$$J_{ntl}\ddot{\theta}_{ntl} + C_{ntl}\dot{\theta}_{ntl} - k_2(\theta_{bg}-\theta_{ntl}) + k_3(\theta_{ntl}-\theta_{tg}) = 0 \quad (9)$$

$$J_{tg}\ddot{\theta}_{tg} + C_{tg}\dot{\theta}_{tg} - k_3(\theta_{ntl}-\theta_{tg}) + k_4(\theta_{tg}-\theta_{tm}) = 0 \quad (10)$$

$$J_{tm}\ddot{\theta}_{tm} + C_{tm}\dot{\theta}_{tm} - k_4(\theta_{tg}-\theta_{tm}) = T_{tm}. \quad (11)$$

REFERENCES

[1] (2016, February) Center for Wind Power Drives. RWTH Aachen. [Online]. Available: https://www.cwd.rwth-aachen.de/1/home/

[2] (2016, February) CENER. National Renewable Energy Centre. [Online]. Available: http://www.cener.com/en/

[3] (2016, February) Fraunhofer IWES. Fraunhofer Institute for Wind Energy and Energy System Technology. [Online]. Available: http://www.iwes.fraunhofer.de/en.html

[4] (2016, February) LORC. Lindoe Offshore Renewables Center. [Online]. Available: http://www.lorc.dk/test-center/lorc-nacelle-testing

[5] (2016, February) Orc catapult. Offshore Renewable Energy Catapult. Formerly the National Renewable Energy Center (narec). [Online]. Available: https://ore.catapult.org.uk/home

[6] (2016, February) NWTC. National Renewable Energy Laboratory National Wind Technology Center. [Online]. Available: http://www.nrel.gov/nwtc/

[7] R. F. Schkoda and C. Fox, "Integration of mechanical and electrical hardware for testing full scale wind turbine nacelles," in *Power Systems Conference (PSC), 2014 Clemson University*, Clemson, SC, March 2014, pp. 1–8.

[8] *IEC 61400-1:2005(E) Wind turbines – Part 1: Design requirements*, Std., Rev. Third edition 2005-08.

This report is available at no cost from the National Renewable Energy Laboratory (NREL) at www.nrel.gov/publications.